www.czasopisma.pan.pl PAN POLSKA AKADEMIA NAUK www.journals.pan.pl

Arch. Metall. Mater. **63** (2018), 1, 315-321

DOI: 10.24425/118943

E. LÓPEZ-MARTÍNEZ*,**#, O. VÁZQUEZ-GÓMEZ***,****,
H.J. VERGARA-HERNÁNDEZ****, B. CAMPILLO*,*****

HYDROGEN ASSISTED CRACKING IN A MICROALLOYED STEEL SUBJECTED TO A RAPID THERMAL CYCLE AT HIGH TEMPERATURE

In a martensitic-bainitic microalloyed steel, the effect of hydrogen on fatigue crack growth was studied using rotary bending fatigue tests. The steel was subjected to a rapid thermal cycle to get a microstructure similar to that which would be formed within the coarse-grained heat-affected zone of a weld. Crack growth was monitored as a function of the number of cycles applied during fatigue tests on three types of specimens: 1) those without hydrogen charge, 2) those charged with hydrogen and 3) those charged with hydrogen which was then discharged through low-temperature heat treatment. All types showed persistent slip marks, and cracks propagated along high-shear-stress planes. In the presence of hydrogen, crack growth was affected by microstructural defects caused by the hydrogen charging process, and the persistent slip marks developed in an area closer to the crack tip and crack path. On the contrary, without hydrogen, crack growth occurred perpendicular to the applied force, and the persistent slip marks were fewer in number and further from the crack tip and crack path. This indicates that the plasticity increased (i.e., the damage that occurred in the presence of hydrogen matched the hydrogen-enhanced local plasticity mechanism).

Keywords: Persistent slip mark, hydrogen enhanced local plasticity, fatigue crack growth, microalloyed steel

1. Introduction

Crack nucleation and crack growth, because of the presence of hydrogen on steel structural components manufactured via welding processes, can be located in the fusion zone (FZ), heat-affected zone (HAZ) or the base material (BM) depending, among other factors, on the hardenability of the BM and the filler material [1-3]. Hydrogen-assisted cracking (HAC) susceptibility can be controlled by selecting the welding design and the microstructure of the BM [4]. The required microstructure is obtained in the BM by controlling the thermo-mechanical processes during the manufacturing process, and it is controlled in the FZ by selecting the filler material and the design of the welding process [4]. In contrast, the microstructure developed in the HAZ can only be controlled by the design of the welding process. Because of this and the nature of the HAZ (residual stresses, susceptible microstructures and microstructural heterogeneities) [1], it is often the welding zone that is most prone to the solubility of hydrogen [2] and therefore also to HAC. Depending on the peak temperatures reached in the HAZ, various subzones can be developed. The coarse-grained HAZ (CGHAZ) is often the most susceptible to HAC. This is because an increase in grain size by dissolution of precipitates leads to a decline in the kinetics of new phase formation by diffusive transformation where, depending on the chemical composition and cooling rate, formation of low-temperature microstructures such as bainite and martensite is possible [5].

Because the thickness of the CGHAZ is often small, it is difficult to determine the mechanical properties and to carry out studies of crack growth behaviour in this subzone [6]. To solve this, studies have been conducted using physical simulations of the thermal cycles experienced in heat-affected subzones in large specimens of such dimension that conventional mechanical tests and other tests to study the mechanical behaviour, hydrogen embrittlement, etc. are possible [7-12].

Crack growth propagation is divided into three stages. Stage I includes the short cracks, Stage II includes the long cracks and Stage III is fracture. In Stage I, a fatigue crack propagates along high-shear-stress planes (45°), and the propagation occurs until it is decelerated by microstructural barriers such as grain boundaries or inclusions, which do not allow the crack to continue in the direction of initial growth. Grain refinement can increase fatigue resistance by inserting a large number of microstructural barriers [13,14]. Stage II begins when the slip starts to develop in various planes near the crack tip because the stress intensity factor increases as a consequence of crack growth. Crack growth

* UNIVERSIDAD NACIONAL AUTÓNOMA DE MÉXICO, FACULTAD DE QUÍMICA, CIUDAD DE MÉXICO, MÉXICO
** UNIVERSIDAD DEL ISTMO, SANTO DOMINGO TEHUANTEPEC, MÉXICO
*** CONSEJO NACIONAL DE CIENCIA Y TECNOLOGÍA, CIUDAD DE MÉXICO, MÉXICO
**** INSTITUTO TECNOLÓGICO DE MORELIA, MORELIA, MÉXICO
***** UNIVERSIDAD NACIONAL AUTÓNOMA DE MÉXICO, INSTITUTO DE CIENCIAS FÍSICAS, CUERNAVACA, MÉXICO
# Corresponding author: edgar0902@comunidad.unam.mx

propagation at this stage is perpendicular to the direction of the applied force. Stage III is related to unstable crack growth. At this stage, crack growth is controlled by static failure modes and is very sensitive to the microstructure, load ratio and stress state.

The effect of hydrogen on crack growth in steels depends on the chemical composition, microstructure and stress state. For example, Marukami and Matsuoka [15] studied the effect of hydrogen in crack growth using rotary fatigue testing in a low-carbon Cr-Mo steel and two austenitic stainless steels (304 and 316). They determined: 1) in the presence of hydrogen, slip bands decrease, resulting in a diminution of the plastic zone, and 2) crack growth occurs perpendicular to the applied force. Furthermore, Fujita et al. [16], using cyclic torsion testing, found that hydrogen increases the observed plasticity by generating additional slip bands in quenched and tempered steel. Additionally, in recent studies, it has been shown that in martensitic steels, plasticity increases, as evidenced by an increase in the formation of slip bands [17].

Two mechanisms have been proposed to explain the possible causes of HAC: hydrogen-enhanced decohesion and hydrogen-enhanced local plasticity (HELP). In the former, hydrogen accumulates at sites such as cracks or interfaces and reduces the force of atomic bonding [18]. In contrast in HELP, two mechanisms have been established: 1) hydrogen facilitates the movement of dislocations by shielding the stress fields on dislocations, and 2) hydrogen promotes plane sliding when it stabilizes edge dislocations [19].

We studied the effect of hydrogen on crack growth in a martensitic-bainitic microalloyed steel subjected to a thermal cycle similar to one that would occur in the CGHAZ during a welding process.

2. Procedure

2.1. Material and thermal treatment

An experimental microalloyed steel with a martensite-bainite microstructure and chemical composition of 0.028% C, 0.244% Si, 1.000% Mn, 0.422% Cr, 0.180% Mo, 1.354% Ni, 0.025% Nb and 0.015% Ti was used. Because the thickness of the HAZ is usually narrow in a weld, it is not possible to obtain samples from this zone for mechanical testing. For this reason, samples of the BM were conventionally heat-treated to reproduce a thermal cycle similar to that experienced in the CGHAZ during welding [8, 11, 20, 21]. Heat treatment of cylindrical specimens (8 mm in diameter by 60 mm in length) was accomplished by austenitization at 1350°C for five minutes followed by a quench in a stirred water bath. The complete thermal cycle that the specimens received is represented in Fig. 1, and it mimicks the thermal cycle of welding with high heat input. The microstructure obtained by this heat treatment was revealed by chemical etching using the LePera reagent.

Fatigue specimens were manufactured from the heat treated specimens using a process similar to that proposed for studying short crack growth [22]. These specimens had less area and two flat faces that were subjected to roughing with SiC sandpaper starting with 600 mesh and progressing through a polishing sequence using alumina at 1-, 0.1- and 0.05-μm particle size. In Fig. 2, the configuration of the specimens is shown.

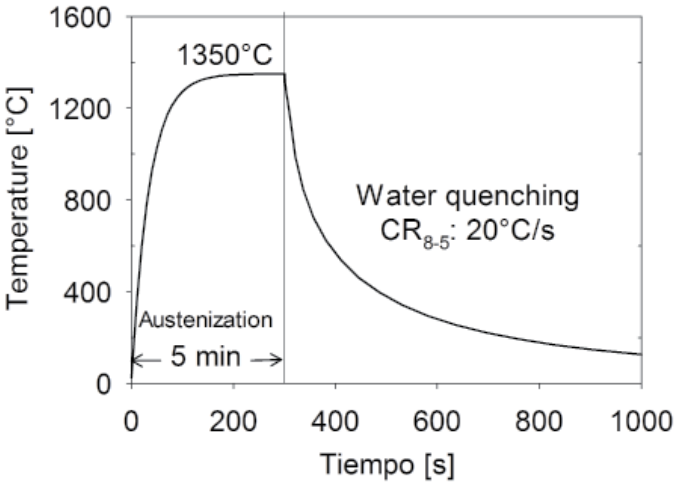

Fig. 1. Thermal cycle to simulate the CGHAZ. $CR_{8\text{-}5}$: cooling rate in the 800 to 500°C temperature range

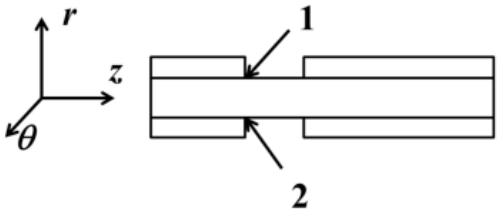

Fig. 2. Modified specimen to study the growth of short cracks. Areas 1 and 2 are designed so that these cracks nucleate in such points. Not drawn to scale

2.2. Fatigue test design

Fatigue tests consisted of determining the bending moment required in the fatigue specimens to assure that it does not exceed the yield stress of the material. Mathematical modelling was applied to elucidate this value. The arrangement of the fatigue test is shown schematically in Fig. 3.

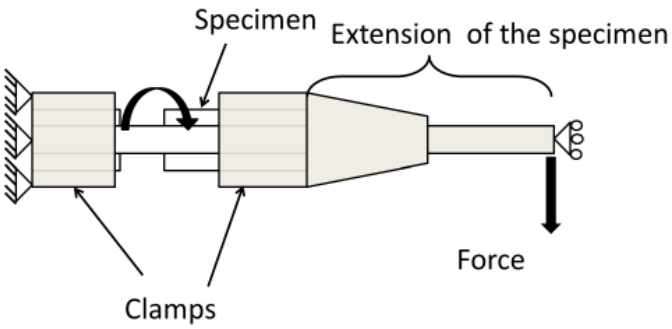

Fig. 3. Drawing of the fatigue test. Not drawn to scale

2.3. Test description

In the fatigue test, a force was applied on the end of the clamp in the fatigue machine, causing a bending moment, and angular movement occurred around the axis of the specimen. The bending moment was of a magnitude that did not exceed the yield stress of the specimen. This process created crack nucleation and crack growth in the stress-concentrating areas that were designed for this purpose (Fig. 2).

2.4. Assumptions

In the mathematical model for the fatigue test, the following assumptions were made:

- Isotropic behaviour
- Ideal elasto-plastic behaviour
- No volume changes in the specimen
- The clamps do not deform either elastically or plastically

2.5. Mathematical formulation

The mathematical formulation of the stress field, regardless of body forces in the fatigue specimen, was determined by a system of differential equations:

$$\sigma_{ij,j} = 0 \tag{1}$$

where σ_{ij} is the stress tensor, and $\sigma_{ij,j}$ is the divergence of this tensor. The free-body diagram of this system and the boundary conditions is shown in Fig. 4.

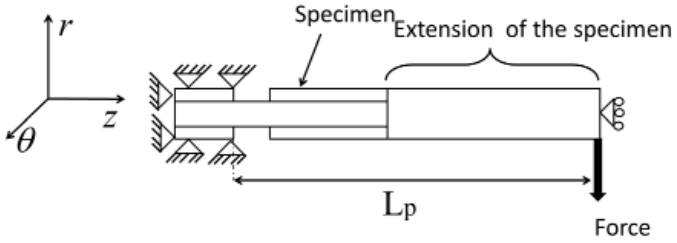

Fig. 4. Scheme of the boundary conditions of the mathematical modeling of fatigue test. L_p is the length from the notch where the crack is expected to nucleate up to the area where the force is applied

2.6. Solving method

To resolve the stress field, the displacement field was determined first using the finite element method, implementing a Lagrangian analysis model using the Abaqus® commercial software package.

To determine the bending moment, in the simulation of the fatigue test, a force was applied in the final part of the extension of the specimen (Fig. 4), and a simulation for such a force was conducted. During post-processing, the applied force was evaluated to determine whether it produced an equivalent plastic strain.

The mechanical properties of the specimens were determined based on an artificial neural network, which was trained and tested in previous work [23].

2.7. Electrochemical hydrogen charging

Fatigue specimens were hydrogen charged using an electrochemical cell with a current density of 40 mA/cm^2 using a graphite anode and a solution of 0.5 M H_2SO_4 with 0.2 g As_2O_3 per litre of solution. Hydrogen was charged for 60 minutes before each fatigue test.

2.8. Fatigue tests

Crack growth was observed using optical microscopy, and it was monitored as a function of the number of cycles applied during the fatigue test on three types of specimens: 1) Type 1 had no hydrogen charge, 2) Type 2 was charged with hydrogen and 3) Type 3 was charged with hydrogen then discharged using a low-temperature thermal treatment. The tests were performed in a rotary fatigue machine (Model RBF 200; Fatigue Dynamics, Inc.), applying a bending moment of 18 lb-in at a frequency of 20 s^{-1}. Type 2 specimens were subjected to a rotary fatigue test immediately upon completion of hydrogen charging. Type 3 specimens were discharged of hydrogen by applying a heat treatment at 150°C for 3 hours before the test was conducted. Following each test, the specimens were attacked with Nital 2 to reveal the microstructure in the crack zone.

3. Results and analyses

The microstructure developed by the thermal cycle is shown in Fig. 5. The LePera reagent dyes the martensite light

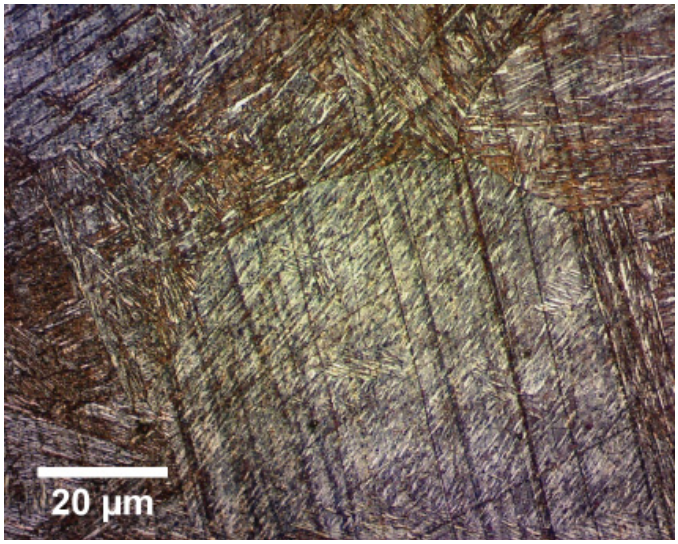

Fig. 5. Microstructure that was developed by the high temperature heat treatment

blue while it dyes the bainite brown [24]. Using quantitative metallography, the microstructure was found to consist of 45% martensite and 55% bainite.

Plastic flow was used to determine the bending moment during fatigue tests, where the applied bending moment did not cause plastic deformation in the notch of the specimen. Figs. 6,7 show the simulation results of equivalent plastic deformations for various values of applied force. When the force was greater than 30 N, it was able to produce plastic flow in the notch area (Fig. 7); therefore, less force is required at this value. Table 1 summarizes the bending moments calculated and used in testing crack growth from rotary fatigue.

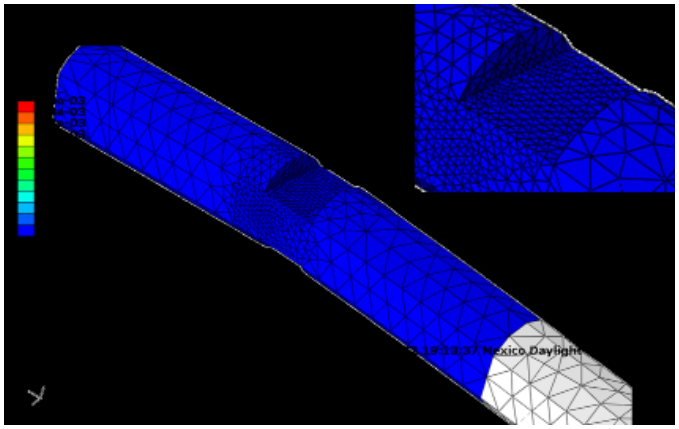

Fig. 6. Equivalent plastic deformation obtained from the fatigue test with an applied bending moment that is equivalent to a force of 30 N

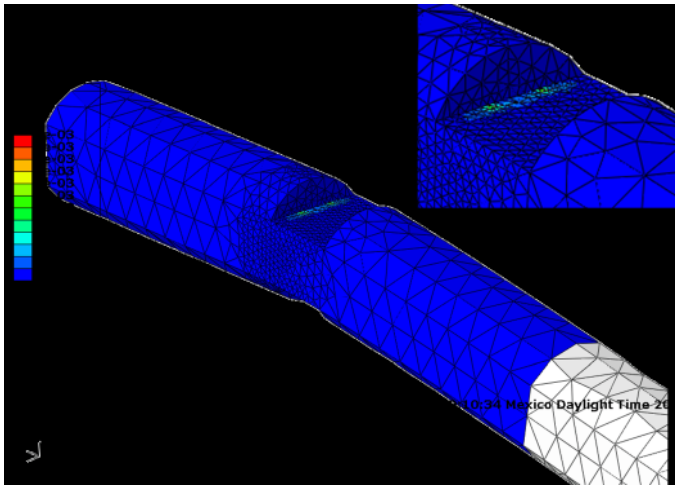

Fig. 7. Equivalent plastic deformation obtained from the fatigue test with an applied bending moment that is equivalent to a force of 40 N

TABLE 1

Bending moment calculated from the force applied in the simulation of the fatigue test and bending moment that was used in the crack growth test for rotary fatigue

Force, N	Length of the extension, mm	Bending moment, N-mm	Bending moment used in the tests, N-mm
30	220	6600	2050

The fatigue tests showed that crack growth originated in the area predicted by numerical simulation, that is, in the notch zone, in the shorter section, which was designed for this purpose. Figs. 8-10 show crack onset for Types 1, 2 and 3, respectively, and the latter two show porosity. All three specimens show persistent slip marks (PSMs), which result from the location of the cyclic plastic deformation in the persistent slip bands (PSBs), which emerge on the surfaces as PSMs. The PSMs consist of extrusions and intrusions, which represent a history of the state of crack formation from fatigue. The initial damage nucleates in grains of the surface along the PSBs in the form of pores or submicron-cracks, on which the plastic deformation is concentrated. During the tension phase, a source of dislocation is activated, and the slip occurs in a preferential direction in a crystallographic plane, where a submicroscopic discontinuity is then formed. This influences another source of dislocation, allowing a new slip to take place along another direction perpendicular to the first slip. When the force is reversed, an indentation formed by the two planes revealed during the tension phase does not disappear, because the slip bands result from plastic deformation. The repetition of tension-compression cycles leads to activation

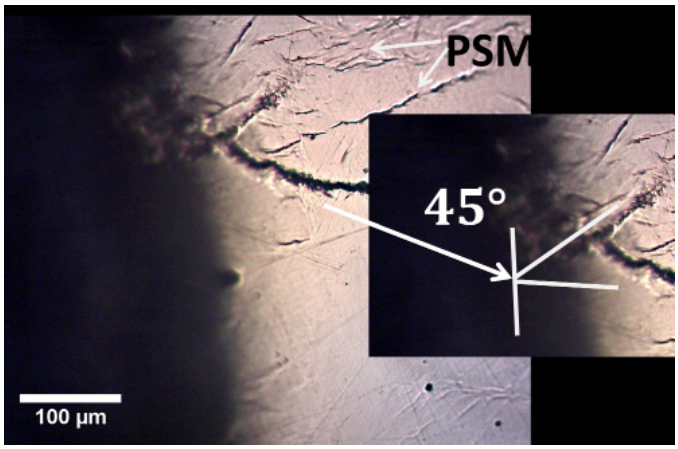

Fig. 8. Start of crack growth. Specimen without charge of hydrogen

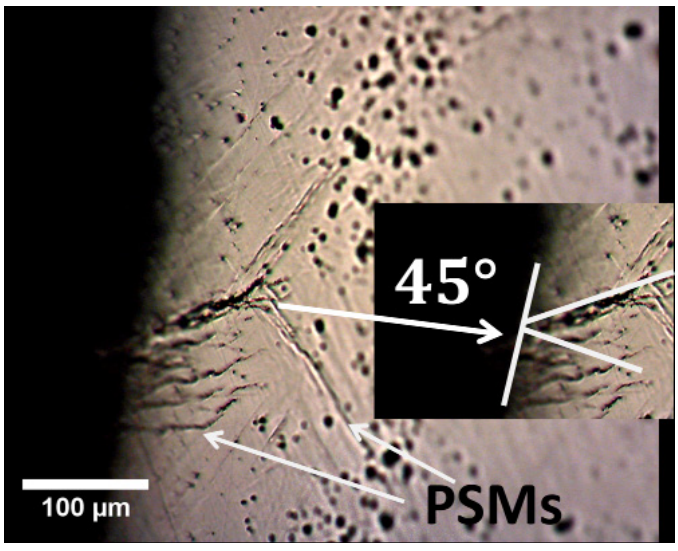

Fig. 9. Start of crack growth. Specimen charged with hydrogen

of new slip bands, and the damage accumulates, eventually generating a micro-crack. Through this mechanism, the crack progressed locally in a zigzag fashion, as shown in Figs. 8-10. In Type 2 specimens (Fig. 9), a greater number of PSMs was observed. In all specimens, fatigue cracks began to propagate along high-shear-stress planes at 45°.

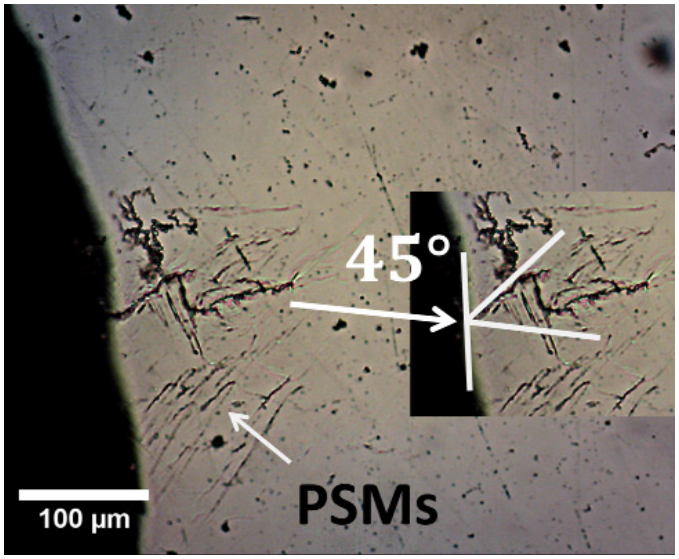

Fig. 10. Start of crack growth. Specimen with charge and discharge of hydrogen

Figs. 11-13 show the crack path with and without chemical etching. These figures show that PSMs continue to develop in areas close to where the crack grows. Additionally, the initial crack is seen to progress in a zigzag path and is approximately as long as the grain diameter, corresponding to a micro-structurally short crack size, although the microstructure continues to affect the crack path as it grows, because the crack develops through inclusions and pores. In Type 1 specimens, crack growth occurred perpendicular to the direction of the applied force, but in Types 2 and 3, crack growth was affected by microstructural defects caused by the hydrogen charge, as seen in Fig. 14 (Type 2), where the crack progressed through the pores that were created. In this specimen, a greater number of PSMs is seen, an indication that the plasticity has increased (i.e., the HELP mechanism was engaged during this damage). Also, PSMs were developed closer to the crack tip and crack path (Fig. 12); however, without hydrogen, the PSMs were fewer in number and located further from the crack tip and crack path (Fig. 11). Fijita et al. [16] and Nagao et al. [17] determined that hydrogen increases plasticity, which is observed through increased slip bands in hardened and tempered steel and in martensitic steel. This is contrary to what has been presented by Marukami and Matsuoka [15], who indicate that in low-carbon Cr-Mo steel with a martensitic microstructure and in the presence of hydrogen, the slip bands decrease, resulting in a diminution of the plastic zone, causing crack growth to occur perpendicular to the applied force. Therefore, various experimental approaches can lead to different conclusions [25].

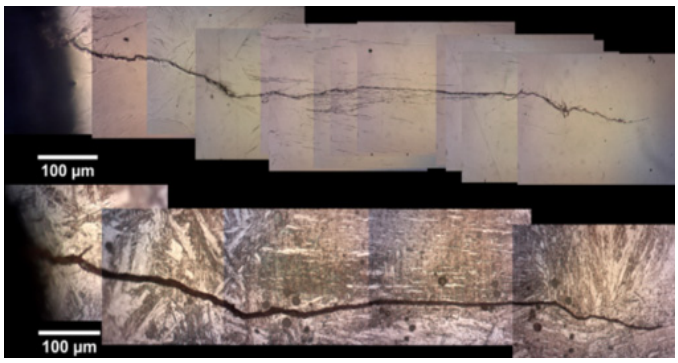

Fig. 11. Crack length developed in the specimen without charge of hydrogen (specimen type 1). a) without etching, b) with etching

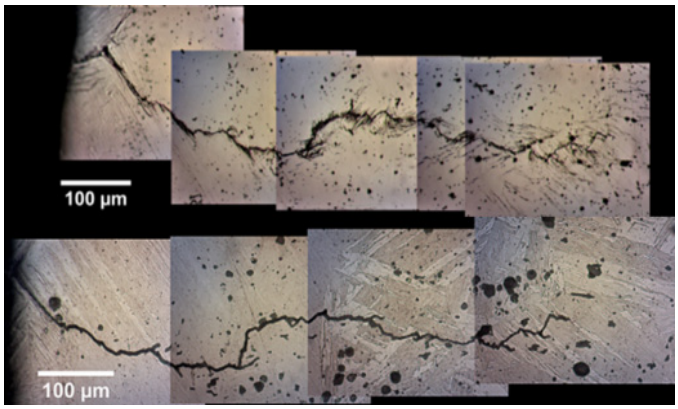

Fig. 12. Crack length developed in the specimen with hydrogen (specimen type 2). a) without etching, b) with etching

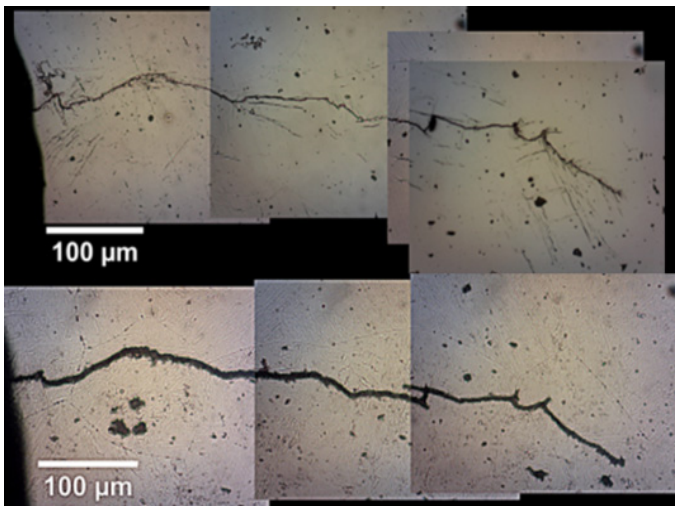

Fig. 13. Crack length developed in the specimen with hydrogen and with discharge treatment (specimen 3). a) without etching, b) etching

Fig. 15 shows the crack length in terms of fatigue cycles, showing that hydrogen affects the number of cycles required to start a crack. In the Type 2 specimen, crack onset was observed at 13,000 cycles, whereas it was at 22,000 cycles in the Type 3 specimen and 40,000 cycles in the Type 1 specimen. In previous work [26], hydrogen traps in the HAZ for this steel are reversible; therefore, in the area of the crack tip, trapped hydrogen (i.e., dif-

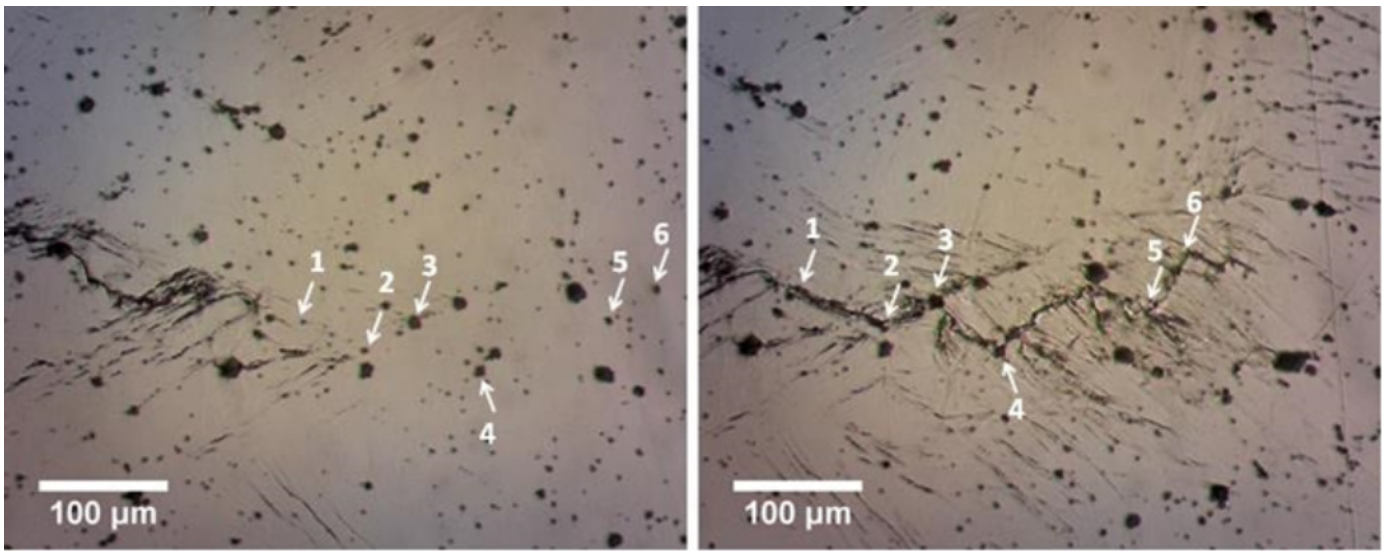

Fig. 14. Progress of the crack on the specimen type 2 (charged with hydrogen). a) 23000 cycles, b) 25500 cycles. The arrows indicate defects where the crack progressed

fusible hydrogen) was released. Hydrogen evidently enabled the onset of crack growth with fewer cycles. In Type 3 specimens, although diffusible hydrogen no longer enabled crack growth in the crack growth zone, the porosity that was developed by the hydrogen charging process caused the crack to grow with fewer cycles. The slope present in Type 2 specimens indicates the effect of hydrogen on crack growth, where the hydrogen came from reversible traps.

Fig. 16 shows a schematic of the mechanism of hydrogen's contribution to crack growth. Hydrogen initially in a reversible trap diffuses to an area where it promotes plasticity in of form of PSB generation on the crack tip through differences in activities (i.e., by the generation of a field of tri-axial stresses in the notch zone of the crack tip). Without hydrogen, a smaller number of PSBs develop, and crack progress decreases.

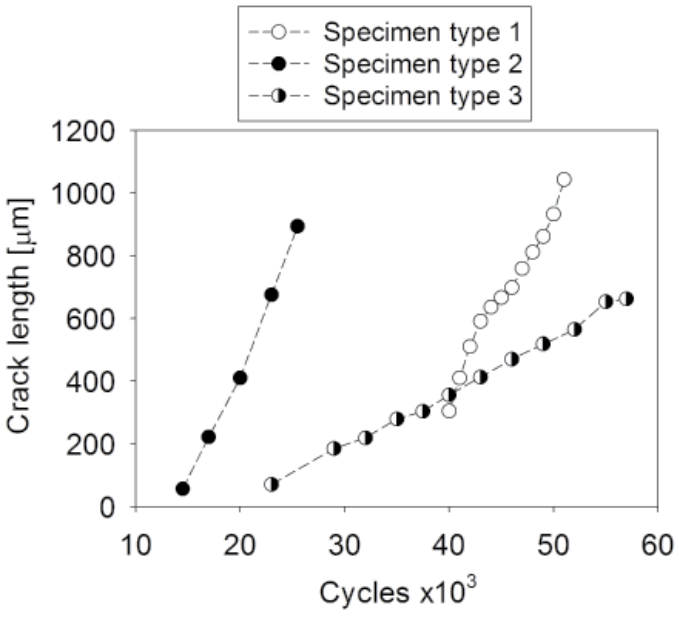

Fig. 15. Crack growth due to fatigue of the three type tested specimens

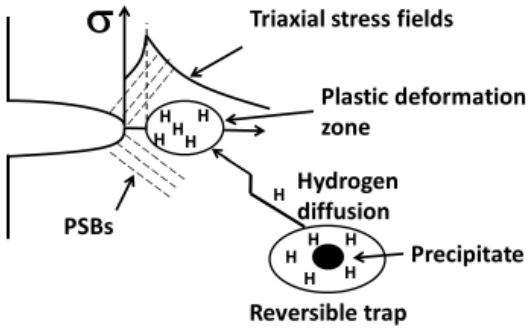

Fig. 16. Scheme of the effect of hydrogen on the crack tip zone

4. Conclusions

The effect of hydrogen on fatigue crack growth was studied in specimens subjected to a thermal cycle similar to the one that occurs in the CGHAZ in a martensitic-bainitic micro-alloyed steel.

In the presence of hydrogen, crack growth is affected by microstructural defects caused by the hydrogen charge, and PSMs develop in an area closer to the crack tip and crack path. On the contrary, without hydrogen, crack growth occurs perpendicular to the applied force, and the PSMs are fewer and located further from the crack tip and from the crack path. This indicates that plasticity increases as a result of hydrogen promoting crack growth, increasing plastic deformation in the area of crack growth, observed as an increase in PSMs. This is consistent with the HELP mechanism.

Acknowledgments

The authors thank the Project Support Program for Research and Technological Innovation under the project IN115616 of the National Autonomous University of Mexico, the National Council of Science and Technology for the

support granted by means of the project of Basic Science SEP-CONACyT 256843 and the Program for Educational Professional Development under the project UNISTMO-PTC-108.

REFERENCES

[1] M.-F. Maday, L. Pilloni, J. Nucl. Mater. **367-370**, 516 (2007).
[2] S.H. Wang, W.C. Luu, K.F. Ho, J.K. Wu, Mater. Chem. Phys. **77**, 447 (2003).
[3] M.A. Smirnov, I.Yu Pyshmintsev, A.N. Maltseva, O.V. Mushina, Metallurgist **56**, 43 (2012).
[4] S. Kuo, Welding Metallurgy, New Jersey 2002.
[5] J.B. Ju, W.S. Kim, J.I. Jang, Mater. Sci. Eng. A. **546**, 258 (2012).
[6] T. Vuherer, P.O. Maruscak, I. Samardzic, Metalurgija **51**, 301 (2012).
[7] C. Li, Y. Wang, T. Han, B. Han, L. Li, J. Mater. Sci. **46**, 727 (2011).
[8] A. Alvaro, V. Olden, A. Macadre, O.M. Akselsen, Mater. Sci. Eng. A **597**, 29 (2014).
[9] H. Dong, X. Hao, D. Deng, Metallogr. Microstruct. Anal. **3**, 138 (2014).
[10] A. Mihi, R. Benbouta, A. Abbassi, R. Cottis, Mater. Corros. **57**, 766 (2006).
[11] A. Moitra, P. Parameswaran, P.R. Sreenivasan, S.L. Mannan, Mater. Charact. **48**, 55 (2002).
[12] Y. Shi, Z. Han, J. Mater. Process. Tech. **207**, 30 (2008).
[13] I. Kubena, B. Fournier, T. Kruml, J. Nucl. Mater. **424**, 101 (2012).
[14] H.W. Höppel, M. Prell, L. May, M. Göken, Procedia Engineering **2**, 1025 (2010).
[15] Y. Murakami, S. Matsuoka, Eng. Fract. Mech. **77**, 1926 (2010).
[16] S. Fujita, S. Matsuoka, Y. Murakami, G. Marquis, Int. J. Fatigue **32**, 943 (2010).
[17] A. Nagao, C.D. Smith, M. Dadfarnia, P. Sofronis, I.M. Robertson, Acta Mater. **60**, 5182 (2012).
[18] V. Olden, C. Thaulow, R. Johnsen, E. Østby, Scripta Mater. **57**, 615 (2007).
[19] I.M. Robertson, Eng. Fract. Mech. **68**, 671 (2001).
[20] K. Homma, C. Miki, H. Yang, Eng. Fract. Mech. **59**, 17 (1998).
[21] M.J. Balart, J.F. Knott, J. Nucl. Mater. **361**, 112 (2007).
[22] K.K. Ray, N. Narasaiah, R. Sivakumar, Mater. Sci. Eng. A **372**, 81 (2004).
[23] E. López Martínez, O. Vázquez Gómez, B.F. Campillo Illanes, Ingeniería mecánica, tecnología y desarrollo **5**, 273 (2014).
[24] E. Girault, P. Jacques, P. Harlet, K. Mols, J. Van Humbeeck, E. Aernoudt, F. Delannay, Mater. Character. **40**, 111 (1998).
[25] N. Saintier, T. Awane, J.M. Olive, S. Matsuoka, Y. Murakami, Int. J. Hydrogen Energy **36**, 8630 (2011).
[26] E. López-Martínez, H.J. Vergara-Hernández, O. Flores, B. Campillo, ISIJ Int. **55**, 2435 (2015).